

Control of the SIRENE Underwater Shuttle: System Design and Tests at Sea.

C. Silvestre A. Aguiar P. Oliveira A. Pascoal

*Institute for Systems and Robotics and Department of Electrical Engineering,
Instituto Superior Técnico, Av. Rovisco Pais, 1096 Lisboa Codex, Portugal
E-mail address: antonio@isr.isr.ist.utl.pt*

Abstract

This paper describes theoretical and practical issues that arose during the development of the control and guidance systems for SIRENE, an autonomous underwater shuttle for the transport and accurate positioning of benthic laboratories in the seabed down to a depth of 4000 meters. The nonlinear hydrodynamic model of the vehicle is described, and a class of sliding mode control laws for vehicle stabilization and steering in the vertical and horizontal planes is derived. The control algorithms are combined with a classical line-of-sight guidance law, and the performance of the resulting system is evaluated in a computer based simulation of a realistic mission scenario. The paper concludes with a description of experimental results obtained during a series of sea tests carried out by the French Agency IFREMER and the Instituto Superior Técnico (IST) off the coast of Toulon, France.

1. Introduction

Recently, there has been renewed interest in the development of stationary benthic stations to carry out experiments on the biology, geochemistry, and physics of deep sea sediments and hydrothermal vents in situ, over long periods of time [13]. However, current methods of deploying and servicing benthic laboratories are costly and require permanent support from specialized crews resident on board manned submersibles or surface ships. See, for example, [5] for a description of the benthic laboratory NADIA II that was first designed for re-entry of deep sea boreholes under the control of a crew stationed on board the 6000 m manned submersible *NAUTILUS*. As a contribution to overcoming some of the abovementioned problems, a European team led by the French Agency IFREMER has developed a prototype autonomous underwater shuttle vehicle named SIRENE to automatically transport and position a large range of stationary benthic laboratories on the seabed down to a depth

of 4000 meters, and service them at a later time. The vehicle was developed in the course of the MAST-II European project DESIBEL (New Methods for Deep Sea Intervention on Future Benthic Laboratories), that aims to compare different methods for deploying and servicing stationary benthic laboratories. The reader is referred to [2] for a general description of the project and to [3] for complete technical details of the work carried out by IFREMER (FR), IST (PT), THETIS (GER), and VWS (GER). This paper de-

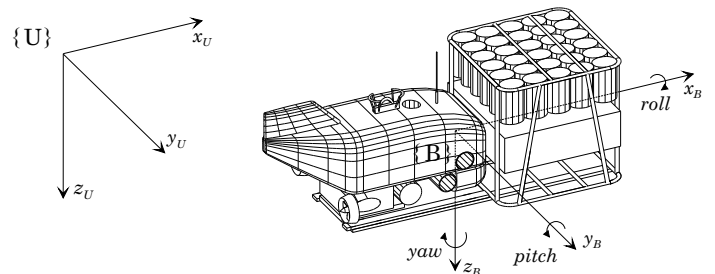


Fig. 1. *SIRENE* coupled to a benthic laboratory. Body-fixed ($\{B\}$) and earth-fixed ($\{U\}$) reference frames.

scribes the research and development work that was carried out by the Instituto Superior Técnico - in the scope of the DESIBEL project - towards the development of the SIRENE guidance and control systems. Design issues are discussed, and practical results obtained with the prototype vehicle at sea are summarized. The first part of the paper focuses on the design of the control and guidance systems of SIRENE to meet strict performance requirements in the presence of uncertain, nonlinear hydrodynamic vehicle dynamics and time-varying currents. A nonlinear hydrodynamic model of the vehicle is described, and a class of sliding mode control laws for vehicle stabilization and steering in the vertical and horizontal planes is derived. The control algorithms are combined with a classical line-of-sight guidance law, and the performance of the resulting system is evaluated in a computer based simulation of a realistic mission scenario. The second part provides a practical counterpart to the theoretical developments presented by summarizing the experimental results on guidance and control that were

¹ This work was supported by the Commission of the European Communities under contract MAS2-CT94-0082 (Project DESIBEL). A. Aguiar received partial support from the Portuguese PRAXIS Programme through a Graduate Student Fellowship.

obtained during a series of sea tests carried out by IFREMER and IST off the coast of Toulon, France.

2. The SIRENE vehicle. Mission scenarios

This section describes the main characteristics of the SIRENE vehicle and summarizes a typical vehicle mission.

2.1 Vehicle characteristics

The SIRENE vehicle - depicted in Fig. 1 - has an open-frame structure and is 4.0 m long, 1.6 m wide, and 1.96 m high. It has a dry weight of 4000 kg and a maximum operating depth of 4000 m. The vehicle is equipped with two back thrusters and one side thruster for surge, sway, and yaw motion control in the horizontal plane, and one vertical thruster for heave control. Roll and pitch motion are left uncontrolled, since the metacentric height² is sufficiently large (36 cm) to provide adequate static stability. In the figure, the vehicle carries a representative benthic lab that was used in this study. The lab is cubic shaped, with a volume of 2.3 m³. In the water and during the final approach to target phase, SIRENE has negative weight and the laboratory has positive weight. The complete ensemble, however, has neutral weight.

2.2 Vehicle mission

The first phase of a typical mission scenario consists of selecting the precise location where the benthic lab will be deployed and marking it with acoustic beacons. SIRENE and the laboratory are then launched from a support ship. During this phase, SIRENE carries a ballast weight. The ensemble starts descending along a free-fall trajectory at a speed in the range from 0.5 to 1 m/s. At approximately 100 m above the seabed SIRENE releases its ballast and the weight of the all ensemble becomes neutral. It is then up to SIRENE to steer the benthic lab to the selected target position, position it on the seabed with a desired heading, and return to the surface. Once deployed, the benthic laboratory will execute a pre-determined plan of experiments over an extended period of time. When required, SIRENE may be instructed to service the laboratory by diving to the exact location of deployment, lock onto the laboratory and recharge its batteries using an electromagnetic energy transmission method.

3. Vehicle Modeling

The dynamic model of the ensemble that consists of SIRENE and the associated laboratory is described next. See [1] for complete details. In what follows, to simplify the presentation, the ensemble will be referred to simply as the vehicle.

3.1 General equations of motion

Following standard practice, the kinematic and dynamic equations of motion of the vehicle can be developed using a global coordinate frame $\{U\}$ and a body-fixed coordinate frame $\{B\}$, as depicted in Figure 1. The following notation is required ([6]):

- $\eta_1 = [x, y, z]^T$ - position of the origin of $\{B\}$ measured in $\{U\}$.
- $\eta_2 = [\phi, \theta, \psi]^T$ - angles of roll (ϕ), pitch (θ), and yaw (ψ) that parametrize locally the orientation of $\{B\}$ with respect to $\{U\}$.
- $\nu_1 = [u, v, w]^T$ - linear velocity of the origin of $\{B\}$ relative to $\{U\}$, expressed in $\{B\}$ (i.e., body-fixed linear velocity).
- $\nu_2 = [p, q, r]^T$ - angular velocity of $\{B\}$ relative to $\{U\}$, expressed in $\{B\}$ (i.e., body-fixed angular velocity).

With this notation, the kinematics and dynamics of the vehicle can be written in compact form as

Kinematics

$$\begin{bmatrix} \dot{\eta}_1 \\ \dot{\eta}_2 \end{bmatrix} = \begin{bmatrix} {}^U_B R(\eta_2) & 0 \\ 0 & Q(\eta_2) \end{bmatrix} \begin{bmatrix} \nu_1 \\ \nu_2 \end{bmatrix} \iff \dot{\eta} = J(\eta)\nu \quad (1)$$

Dynamics

$$M_{RB}\dot{\nu} + C_{RB}(\nu)\nu = \tau_{RB} \quad (2)$$

where ${}^U_B R(\eta_2)$ is the rotation matrix from $\{B\}$ to $\{U\}$ parameterized by the vector η_2 of roll, pitch, and yaw angles, and $Q(\eta_2)$ is the matrix that relates body-fixed angular velocity with roll, pitch, and yaw rates. The vector $\nu = [u, v, w, p, q, r]^T$ consists of the body-fixed linear and angular velocity vectors, and $\tau_{RB} = [X, Y, Z, K, M, N]^T$ is the generalized vector of external forces and moments. The symbols M_{RB} and C_{RB} denote the rigid body inertia matrix and the matrix of Coriolis and Centrifugal terms, respectively. The vector τ_{RB} can further be decomposed as $\tau_{RB} = \tau + \tau_A + \tau_D + \tau_R$, where τ_R denotes the term due to buoyancy and gravity, and τ_A is the added mass term. The term τ_D captures the damping and lift effects, and τ represents the forces and moments generated by the thrusters. The following notation is also used in the text:

² distance between the center of buoyancy and the center of mass.

$\alpha = \arcsin(w/(u^2 + w^2)^{1/2})$ is the angle of attack, and $\beta = \arcsin(v/(u^2 + v^2 + w^2)^{1/2})$ is the angle of sideslip.

3.2 System identification. Hydrodynamic tests

To be of practical use, the general equations of motion must be tuned for the vehicle in study. The main difficulty lies in computing the term τ_{RB} that arises in the dynamics equation. In the present case, this was done using both theoretical and experimental methods, and by exploring the analogy with similar existing vehicles.

The restoring term τ_R was easily computed from geometrical considerations. The added mass term was decomposed as $\tau_A = -M_A \dot{\nu} - C_A(\nu)\nu$, where M_A and $C_A(\nu)$ were determined by analogy with the *Dolphin 3K* vehicle assuming that M_A was diagonal. Following [8], the forces and moments that act on the vehicle due to viscous effects caused by skin friction and quadratic drag due to vortex shedding were assumed to be of the form $\tau_D = [\tau_{D_1}^T, \tau_{D_2}^T]^T$, where

$$\tau_{D_1} = \frac{1}{2} \rho \nabla^{\frac{2}{3}} V_r^2 \begin{bmatrix} C_X(\alpha, \beta) \\ C_Y(\alpha, \beta) \\ C_Z(\alpha, \beta) \end{bmatrix} + \begin{bmatrix} X_{|p|p}|p|p \\ Y_{|r|r}|r|r \\ Z_{|q|q}|q|q \end{bmatrix} \quad (3)$$

$$\tau_{D_2} = \frac{1}{2} \rho \nabla V_r^2 \begin{bmatrix} C_K(\alpha, \beta) \\ C_M(\alpha, \beta) \\ C_N(\alpha, \beta) \end{bmatrix} + \begin{bmatrix} K_{|p|p}|p|p \\ M_{|q|q}|q|q \\ N_{|r|r}|r|r \end{bmatrix} \quad (4)$$

In the equations, ρ is the density of the water, V_r is the absolute value of the velocity of the vehicle with respect to the water, and ∇ is the volume of fluid displaced by the vehicle. Equations (3) and (4) can be rewritten as $\tau_D = -D(\nu)\nu$, where the hydrodynamic damping matrix $D(\nu)$ is strictly positive [6]. In order to estimate some of the parameters in

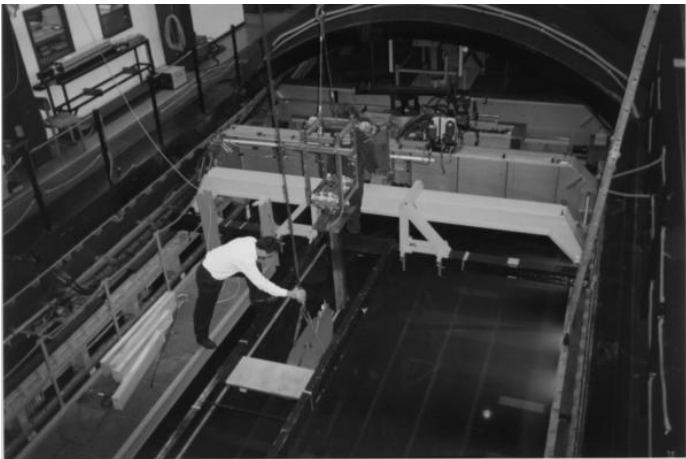


Fig. 2. Hydrodynamic tests preparation: positioning the model in the circulating water channel.

the above equations, a series of tests were performed in a circulating water channel at the *VWS - Versuchsanstalt für Wasserbau und Schiffbau*, Berlin (see Fig. 2) with a quarter scale model of the vehicle. The non-dimensional drag coefficients of the model in the three directions of motion are given by $X'_{|u|u} = -0.57$, $u > 0$; $Y'_{|v|v} = -1.09$, $v < 0$; $Z'_{|w|w} = -1.0$, $w < 0$. From the test results, it was concluded that there is no dependence of the hydrodynamic coefficients on the Reynolds number in the velocity range from $0.5 - 1$ m/s. Since no dynamic tests were performed, the coefficients in equations (3), (4) were determined using the reduced set of test data, and by establishing an analogy with the *Dolphin 3K* vehicle [8]. Figure 3 shows some of the estimated parameters.

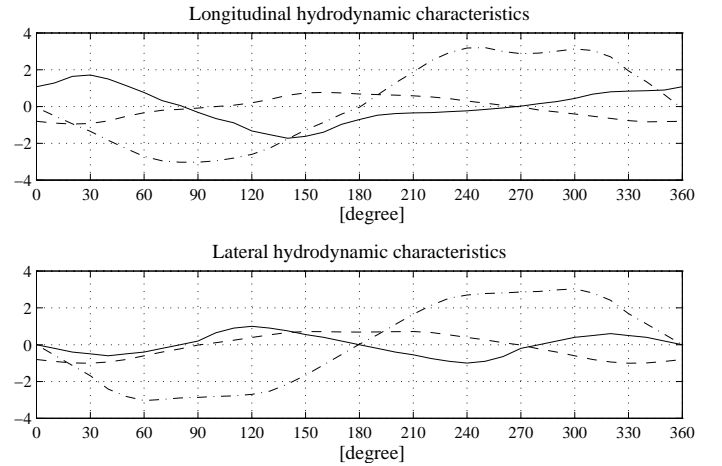


Fig. 3. Hydrodynamic characteristics of the vehicle.

3.3 Equations of motion: compact notation

Combining equations (1) and (2) the 6 DOF body-fixed vehicle equations of motion can be written in compact form as

$$M \dot{\nu} + C(\nu)\nu + D(\nu)\nu + g(\eta) = \tau \quad (5)$$

$$\dot{\eta} = J(\eta)\nu$$

where τ is the vector of actuator control forces and moments, $g(\eta) = -\tau_R$, $M = M_{RB} + M_A$, and $C(\nu) = C_{RB}(\nu) + C_A(\nu)$. It is assumed that M is constant and positive definite, and that $C(\nu)$ is skew-symmetrical, i.e., $M = M^T > 0$, $\dot{M} = 0_{6 \times 6}$, and $C(\nu) = -C^T(\nu)$.

4. Control system design

4.1 System requirements. Control strategies.

Following the discussion in section 2.2, two basic maneuvers were defined for control system design purposes (see Fig. 4):

- Flight maneuver - transition from free-fall to the fine positioning phase: the vehicle is required to follow a pre-determined trajectory to arrive at a neighborhood of the final target.
- Fine positioning maneuver - final approach and landing on a target site.

During flight maneuvers, only the vertical and the two main back thrusters are enabled. Therefore, there are a smaller number of actuators than degrees of freedom to be controlled. To tackle this problem, it was decided to design separate controllers for speed, heading, and depth and to leave roll and pitch passive. This procedure is often used in practice and leads to good results in the case where the meta-centric height is large and there is little interaction between the different vehicle motions [7]. Following this approach, the control variables used in the speed, heading, and depth control loops are the common mode and differential mode activity of the back thrusters, and the activity of the vertical thruster, respectively. Tracking of a reference path in the horizontal plane can be achieved by combining the control loops for speed and heading with a simple line-of-sight guidance scheme [7]. During fine positioning maneuvers, all the thrusters (including the lateral) are enabled and the vehicle becomes fully actuated in the horizontal plane.

Control system design addressed the problems of vehicle stabilization and precise command following in the presence of large vehicle and actuator hydrodynamic parameter uncertainty. The importance of this issue can be hardly overemphasized, since it was expected that some of the hydrodynamic parameters would differ by as much as 50% from their estimated values. The methodology adopted for control system design borrows from sliding mode control theory, and leads naturally to a controller structure that exhibits proportional, derivative, and integral terms, together with additional nonlinear terms that provide robustness against vehicle parametric uncertainty. The reader is referred to [4], [14] for in-depth presentations of sliding mode control theory, and to [6], [7], [15] for interesting applications in the area of underwater robotics. The next section describes the structure of the controllers for the SIRENE vehicle. Due to space limitations, only the algorithms for heading and depth control are briefly reviewed. See [1] for complete details on control system design based on the techniques described in [12].

4.2 Heading and Depth Control

Simplified equations of motion. From (5), the simplified equations of motion for heading and depth can be written as [6]

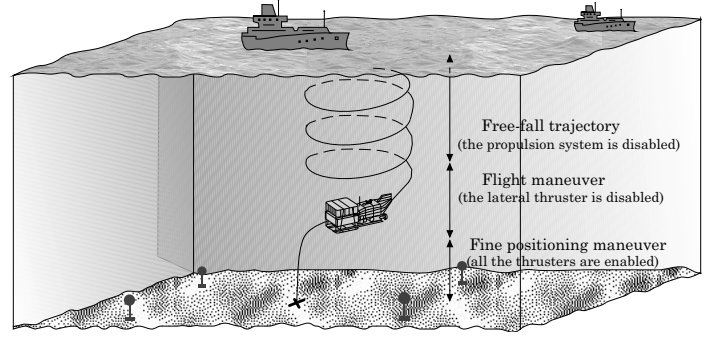


Fig. 4. Mission scenario.

$$(I_{zz} - N_{\dot{r}})\ddot{\psi} - N_{|r|r}|\dot{\psi}|\dot{\psi} + h_{\psi}(t) + \tilde{d}_{\psi}(t) = u_{\psi}$$

$$(m - Z_{\dot{w}})\ddot{z} - Z_{|w|w}|\dot{z}|\dot{z} + (B - W) + h_z(t) + \tilde{d}_z(t) = u_z$$

where $h_{\psi}(t)$ and $h_z(t)$ represent neglected nonlinear coupling terms and unmodeled dynamics, u_{ψ} and u_z are the external torque due to the main thruster differential activity and the force provided by the vertical propulsion, respectively, and $\tilde{d}_{\psi}(t)$ and $\tilde{d}_z(t)$ denote external disturbances such as those generated by currents. Each of the two equations can be rewritten in compact form as

$$m^* \ddot{\chi} + d^* \dot{\chi} + g^* + h^* + \tilde{d}^* = u^*, \quad (6)$$

where χ denotes the variable ψ or z , and m^* and $d^* = d^*(\dot{\chi})$ are positive real numbers.

Sliding mode control laws. Let \hat{m}^* , \hat{d}^* , \hat{g}^* , and \hat{h}^* be the nominal values of the corresponding variables in (6), and suppose that the following assumptions apply:

Assumption 1. The desired trajectory χ_d and its derivatives up to order two are continuous and bounded.

Assumption 2. The parameter uncertainties $\Delta m^* = \hat{m}^* - m^*$, $\Delta d^* = \hat{d}^* - d^*$, and $\Delta g^* = \hat{g}^* - g^*$ satisfy $|\Delta m^*| \leq \delta_{\Delta m^*}$, $|\Delta d^*| \leq \delta_{\Delta d^*} |\dot{\chi}|$, and $|\Delta g^*| \leq \delta_{\Delta g^*}$, where the values of $\delta_{\Delta m^*}$, $\delta_{\Delta d^*}$, and $\delta_{\Delta g^*}$ are constant and known a priori.

Assumption 3. The term $\Delta h^* = \hat{h}^* - h^*$ and the external perturbation $\tilde{d}^*(t)$ satisfy $|\Delta h^*| \leq \delta_{\Delta h^*} |\dot{\chi}|$ and $|\tilde{d}^*(t)| \leq \delta_{d^*}$, where $\delta_{\Delta h^*}$ and δ_{d^*} are constant and known a priori.

Following the methodology in [12], consider the function s defined by $e = \chi - \chi_d$; $s = \dot{e} + \lambda e = \dot{\chi} - \dot{\chi}_d$, where λ is a positive number. The following control law is used:

$$u^* = \begin{cases} \hat{m}^* \ddot{\chi}_r + \hat{d}^* \dot{\chi}_r + \hat{g}^* + \hat{h}^* - k \operatorname{sgn}(s) \\ -k_D s \\ \hat{m}^* \ddot{\chi}_r + \hat{d}^* \dot{\chi}_r + \hat{g}^* + \hat{h}^* - \frac{1}{\epsilon} k s \\ -k_D s - k_I \int_{t_c}^t s(\tau) d\tau \end{cases} \quad \begin{array}{l} |s| > \epsilon \\ |s| \leq \epsilon \end{array} \quad (7)$$

where k , k_D , and k_I are positive scalars.

Close inspection of the sliding mode controller structure reveals the existence of two distinct regions of operation separated by the boundary $|s| = \epsilon$. Outside the boundary layer, the controller contains terms that cancel the nominal nonlinear dynamics of the vehicle, together with a term proportional to s and a switching term aimed at providing robustness against parametric uncertainty. Inside the boundary layer, the controller contains an additional integral term that aims at achieving zero steady-state error in response to constant commands.

The stability of the control scheme adopted follows from the results in [1], where it is shown that: *i*) the boundary is reached in finite time, and *ii*) for any constant input command, the variable s (and therefore the tracking error e) converge to zero.

4.3 Guidance system: effects of ocean currents

The purpose of the guidance system is to generate references for the vehicle control systems so as to achieve adequate tracking of trajectories specified in a universal reference frame. This requirement is important during the execution of flight maneuvers aiming at transferring the vehicle to the vicinity of the final target location.

Way Point Guidance by Line of Sight (LOS). The guidance law used in this study is similar to that described in [7]. Suppose that a flight maneuver is defined by a finite sequence of way points (x_k, y_k, z_k) : $k = 1, \dots, N$. Assuming that the vehicle progresses at constant speed and that the depth coordinate is controlled independently, the line of sight guidance scheme computes reference commands

$$\psi_r(t) = \tan^{-1} \left(\frac{y_k - y(t)}{x_k - x(t)} \right) \quad (8)$$

where the value of k is incremented when the vehicle reaches a *circle of acceptance* with radius ρ_0 centered at the next way point, i.e. when the vehicle location $(x(t), y(t))$ is such that

$$\rho^2(t) = [x_k - x(t)]^2 + [y_k - y(t)]^2 < \rho_0^2$$

Notice that in equation (8) care must be taken to select the proper quadrant for ψ_r .

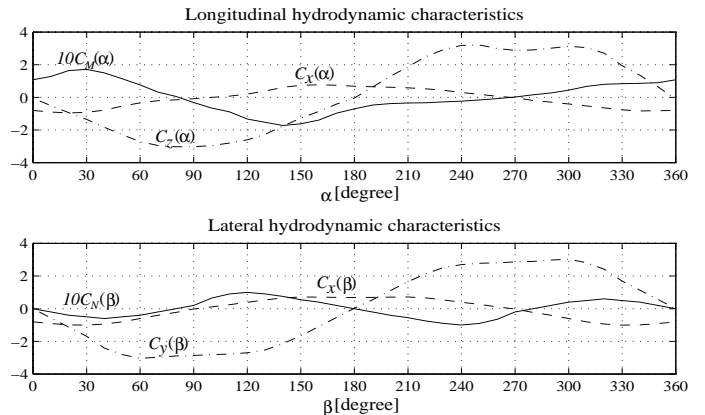


Fig. 5. Way point guidance: line of sight (LOS); current velocity: $U \nu_w = [-0.3, 0, 0]^T$ m/s.

Effects of Ocean Currents. In the presence of ocean currents and when the vehicle is executing flight maneuvers at slow speed, trajectory tracking performance may degrade significantly. This is illustrated in Fig. 5, which shows the results of a simulation where the current is $U \nu_w = [-0.3, 0, 0]^T$ m/s and the reference for linear position is a planar square wave shaped trajectory defined by the way points $(x_0, y_0) = (0, 0)$ m, $(x_1, y_1) = (200, 0)$ m, $(x_2, y_2) = (200, 200)$ m, $(x_3, y_3) = (0, 200)$ m, $(x_4, y_4) = (0, 400)$ m, $(x_5, y_5) = (200, 400)$ m, ... The forward speed command was held constant at 0.5 m/s.

In order to improve performance under current perturbations, a current compensation for the heading autopilot was developed. Since SIRENE is equipped with a Doppler unit that provides measurements of the linear position rates \dot{x} , \dot{y} , the key idea is to align the total vehicle velocity direction with the command for heading - issued by the guidance scheme - by acting on the back thrusters in differential mode. This can be done by redefining the tracking error as $e = \psi' - \psi_r$, where $\psi' = \tan^{-1} \left(\frac{\dot{y}}{\dot{x}} \right)$. Again, care must be taken to select the proper quadrant for ψ' . Figure 6 shows the performance of the control law with current compensation.

5. Mission simulation

To assess the performance of the controllers in the presence of parametric uncertainty and unforeseen sea currents, a computer simulation was performed of a typical benthic laboratory deployment mission.

Mission Requirements. The objective is to deploy the benthic lab at $(x, y, z) = (0, 0, 1100)$ m with heading $\psi = 0^\circ$. The mission is split into five phases:

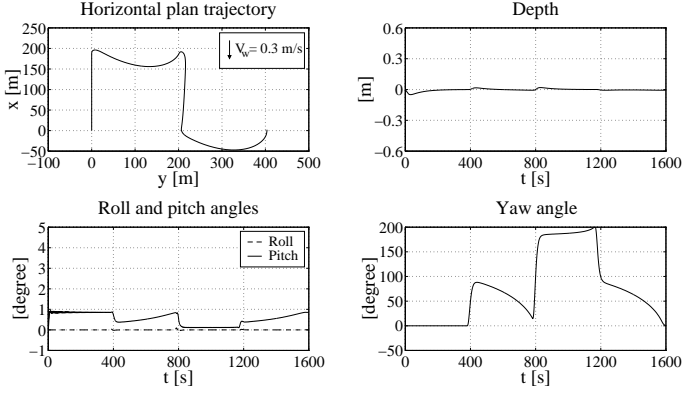


Fig. 6. Way point guidance: line of sight (LOS) with current compensation; current velocity: $U_{\nu_w} = [-0.3, 0, 0]^T$ m/s.

- (1) Submerge - The vehicle descends with all the thrusters disabled, under the action of a ballast with mass $m \simeq 200$ kg.
- (2) Ballast release - This phase is activated when the vehicle reaches the altitude of 100 m above the sea bottom. The ballast is dropped, and the vehicle becomes nearly neutrally buoyant. It then remains inactive for three minutes, in order to damp out the oscillations in pitch that were triggered by the ballast release.
- (3) Flight maneuver - The vehicle progresses at speed $u_d = 0.5$ m/s and transits from its initial position to the way point $(x_1, y_1, z_1) = (0, 0, 100)$ m. The radius of acceptance ρ_0 is 25 m.
- (4) Fine positioning maneuver - The vehicle is steered to the final target position. The desired reference for linear position is $(x_d, y_d, z_d) = (0, 0, 1100)$ m and that for heading is 0° .
- (5) Return - SIRENE releases the benthic lab and returns to the surface. Free ascent is possible, since SIRENE has now a total negative weight.

Simulation Results. Figures 7, 8, and 9 show the simulation results. The vehicle starts at the initial position $(x_0, y_0, z_0) = (0, 0, 0)$ m with orientation $(\phi_0, \theta_0, \psi_0) = (0^\circ, -7.5^\circ, 0^\circ)$. The value of $\theta_0 = -7.5^\circ$ corresponds to the equilibrium point that is achieved at zero speed, when SIRENE is attached to the benthic lab and has a ballast of $m = 200$ kg. In the simulation, a uniform constant current with a velocity amplitude of $V_w = 0.1$ m/s and heading $\psi = 135^\circ$ was considered. All the vehicle parameters were disturbed by 50 % from their nominal values. Furthermore, all commands inputs were pre-filtered by a 3rd-order filter in order to smooth accelerations in response to step input commands [1]. The figures illustrate the first four phases of the mission. Phase 1 (submerge) ends at $t = 1874$ s, when the vehicle reaches the depth of 1000 m. Fig. 8 shows that the verti-

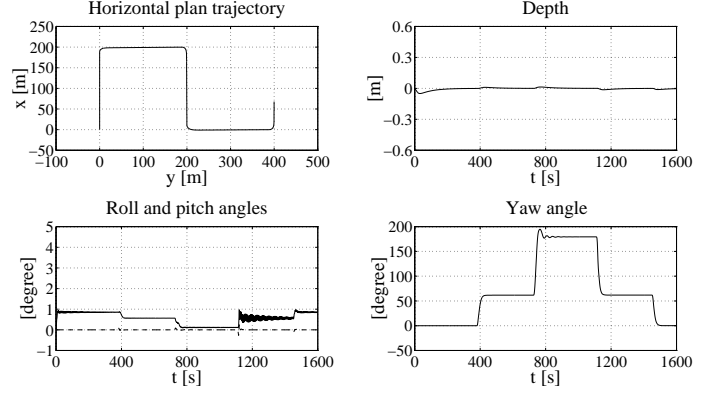


Fig. 7. Vehicle trajectory. Mission performed: positioning the benthic lab at $(x, y, z) = (0, 0, 1100)$ m with heading $\psi = 0^\circ$. There is a constant uniform horizontal current of intensity $V_w = 0.1$ m/s and heading $\psi_w = 135^\circ$, i.e., $U_{\nu_w} = [\dot{x}_w, \dot{y}_w, \dot{z}_w]^T = [-0.07, 0.07, 0]^T$ m/s.

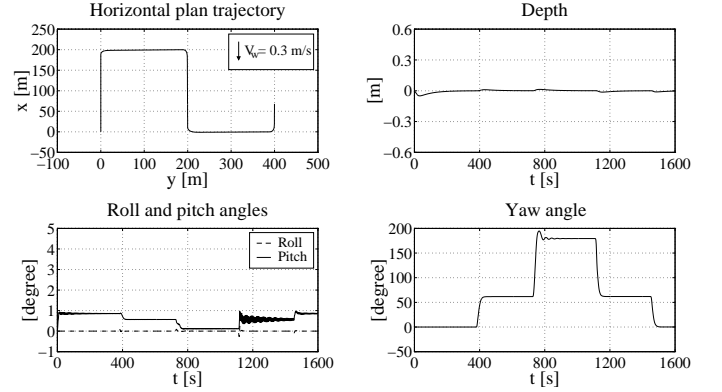


Fig. 8. Linear body-fixed velocity, angle of attack (α), and angle of sideslip (β).

cal velocity w is approximately 0.5 m/s and drops to zero when the ballast is released. Phase 2 is easily identified by the damped oscillatory behavior of the pitch angle in Fig. 9, which converges to the new equilibrium point $\theta = 0^\circ$. Three minutes into phase 2, i.e. at $t = 2054$ s, phase 3 starts. As shown in the simulation, forward speed u goes to 0.5 m/s as desired, depth is kept about 1000 m, and heading goes to $\psi \simeq -64^\circ - 6 \times 360^\circ = -2224^\circ$. Notice that the vehicle had to turn approximately 170° because, when the control and guidance system were activated, the value of heading was $\psi \simeq 106^\circ - 6 \times 360^\circ = -2054^\circ$ (i.e. the vehicle was pointing in a direction that was almost opposite to that commanded); see figs. 7 and 9. At $t = 2283$ s, the vehicle reaches the required way point neighborhood. At that moment, the control system switches to the fine positioning maneuvering mode. The lateral thruster is now enabled (see Fig. 9) and the ensemble is positioned on the final target.

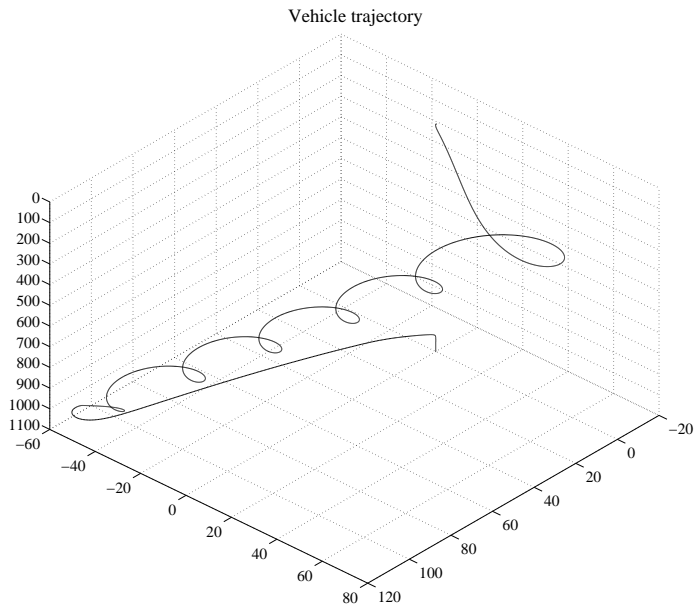


Fig. 9. *Vehicle translational and rotational motion responses. Controller activity.*

6. Experimental Results

The simulation study in Section 5 indicated that the types of control strategies developed were good candidates for real world applications. However, further work was required to transition from theory to practice and to actually implement the strategies developed on the computers installed on-board the SIRENE vehicle. In particular, the problem of control system re-design in the absence of full state information had to be addressed and solved. This was done by simplifying the structure of the sliding mode controllers while retaining some of the nonlinear terms for robustness purposes. In the re-design process, the original sliding mode controllers played the role of benchmarks against which to compare the performance achieved with the new ones. Due to space limitations, this issue is not addressed here; see [10] for complete details on the implementation of the control and guidance systems adopted, as well as a description of the hardware and software architectures for vehicle and mission control. See also [10] for a description of the main mission control tasks using Petri net models [9]. During the period from June until December 1997, a series of tests were carried out with SIRENE and a mock-up of a benthic laboratory off the coast of Toulon, France that culminated with the landing of the vehicle in an autonomous mode at a depth of approximately 2000 meters. Figures 10, 11, 12 and 13 are but a small sample of the large amounts of experimental data that were obtained in the course of the test programme [10]. Figures 10 and 11 show commanded

and measured heading and depth, respectively. Figures 12 and 13 show the response of the vehicle to step commands in the inertial coordinates x and y . In the results shown, the vehicle positioning system relied on information provided by a long baseline system (LBL) and on vehicle thruster data. However, it did not use the Doppler unit to smooth out the position estimates between LBL updates. This explains the discontinuities observed in the *measured positions*.

7. Conclusions

The paper described the design and testing of the guidance and control systems of SIRENE, an autonomous underwater shuttle for the transport and precise positioning of benthic laboratories at a depth of 4000 meters. The results obtained have paved the way for the development of a future

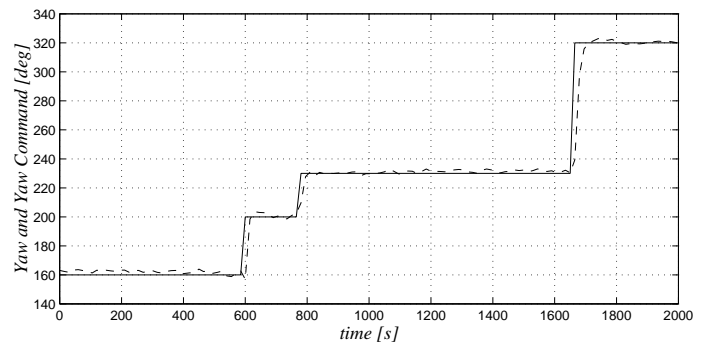


Fig. 10. *Commanded and measured yaw angle.*

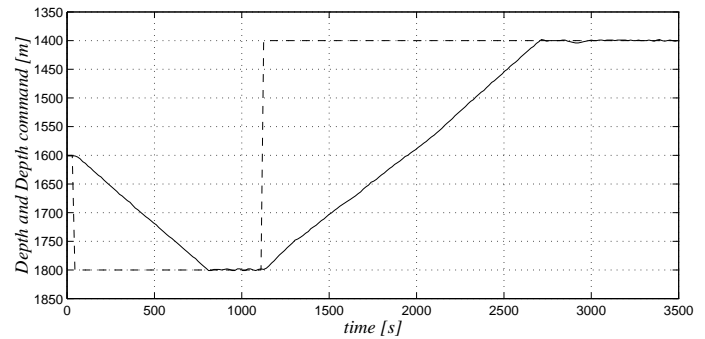


Fig. 11. *Commanded and measured depth.*

generation of underwater shuttles that will endow end-users with the capability to automatically deploy and service a large range of benthic laboratories; Future research issues will address the problems of precise control of position and heading of the shuttle in the absence of lateral thrusters and the development of advanced navigation and control laws for shuttle / benthic docking during servicing operations.

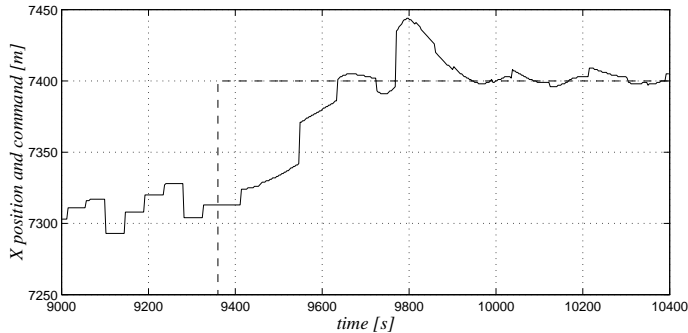


Fig. 12. Commanded and measured X position.

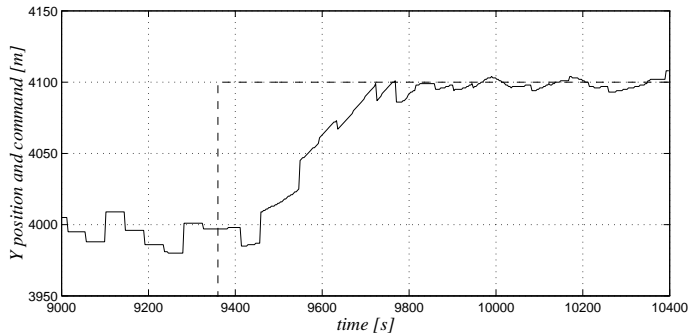


Fig. 13. Commanded and measured Y position.

Acknowledgment

The authors are indebted to V. Goetz from VWS, Germany for the results of the hydrodynamic tank tests. The advice and technical expertise of Laurent Brisset, Vincent Rigaud, and Dominique Semac of IFREMER during all phases of the project BENLAB were truly appreciated. Finally, our warmest thanks to Manuel Rufino, Luis Sebastiao, and Victor Silva who collaborated in the development of software and hardware equipment and provided valuable assistance during the sea trials.

8. References

- [1] A. Aguiar. *Modeling, Control, and Guidance of an Autonomous Underwater Shuttle for the Transport of Benthic Laboratories*. MSc. Thesis. Dept. Electrical Engineering, IST, Lisboa, Portugal, 1996.
- [2] L. Brisset, M. Nokin, D. Semac, H. Amann, W. Shneider, and A. Pascoal. *New methods for deep sea intervention on future benthic laboratories: analysis, development, and testing*, in Proc. Second Mast Days and Euromar Market, pp. 1025-1037, Sorrento, Italy, 1995.
- [3] L. Brisset. *DESIBEL project - Technical Report*, IFREMER, France, December 1995.

- [4] R. DeCarlo, S. Zak, and G. Matthews. Variable structure control of nonlinear multivariable systems: a tutorial, *IEEE Proceedings*, 76(3):212–232, April 1988.
- [5] L. Flourey and R. Gable. The technology for wireline re-entry of deep ocean boreholes employed for the Dianaut program, *Geophysical Research Letters*, volume 19, No.5, pp. 497–500, March 1992.
- [6] T. Fossen. *Guidance and Control of Ocean Vehicles*. John Wiley & Sons, England, 1994.
- [7] A. Healey and D. Lienard. Multivariable sliding mode control for autonomous diving and steering of unmanned underwater vehicles, *IEEE Journal of Oceanic Engineering*, OE-18(3):327–339, July 1993.
- [8] M. Nomoto and M. Hattori. The deep ROV DOLPHIN 3K : design and performance analysis, *IEEE J. Oc. Engineering*, OE-11(3):373–391, July 1986.
- [9] P. Oliveira, A. Pascoal, V. Silva, and C. Silvestre. Design, development, and testing of a mission control system for the MARIUS AUV, to appear in *International Journal of Systems Science*, 1998.
- [10] A. Pascoal, P. Oliveira, and C. Silvestre. *DESIBEL project Final Technical Report*, IST, Portugal, December 1997.
- [11] C. Silvestre. *Modeling and Control of Autonomous Underwater Vehicles*. MSc. Thesis. Dept. Electrical Engineering, IST, Lisboa, Portugal, 1991.
- [12] J.J. E. Slotine and W. Li. *Applied Nonlinear Control*. Prentice-Hall, New Jersey, 1991.
- [13] H. Tiel et al. Scientific requirements for an abyssal benthic laboratory, *Journal of Marine Systems* 4, pp. 421–439, 1994.
- [14] V. I. Utkin. *Sliding Modes and Their Application to Variable Structure Systems*. MIR Publishers, Moscow, 1978.
- [15] D. Yoerger, and J.J. Slotine. Robust trajectory control of underwater vehicles, *IEEE Journal of Oceanic Engineering*, OE-10(4):462–470, October 1985.